Wright State University
CORE Scholar

Browse all Theses and Dissertations | Theses and Dissertations

2015

Correlations Between Sensory Encoding and Central Morphology of Muscle Proprioceptors in the Rat

Hanna Marie Gabriel
Wright State University

Follow this and additional works at: https://corescholar.libraries.wright.edu/etd_all

 Part of the Neuroscience and Neurobiology Commons, and the Physiology Commons

Repository Citation

Gabriel, Hanna Marie, "Correlations Between Sensory Encoding and Central Morphology of Muscle Proprioceptors in the Rat" (2015). *Browse all Theses and Dissertations*. 1297.
https://corescholar.libraries.wright.edu/etd_all/1297

This Thesis is brought to you for free and open access by the Theses and Dissertations at CORE Scholar. It has been accepted for inclusion in Browse all Theses and Dissertations by an authorized administrator of CORE Scholar. For more information, please contact library-corescholar@wright.edu.

CORRELATIONS BETWEEN SENSORY ENCODING AND CENTRAL MORPHOLOGY OF MUSCLE PRORIOCEPTORS IN THE RAT

A thesis submitted in partial fulfillment of the
requirements for the degree of
Master of Science

By

Hanna Marie Gabriel
B.A., The College of Wooster, 2013

2015
Wright State University

WRIGHT STATE UNIVERSITY

GRADUATE SCHOOL

May 21, 2015

I HEREBY RECOMMEND THAT THE THESIS PREPARED UNDER MY SUPERVISION BY Hanna Marie Gabriel ENTITLED Correlations between sensory encoding and central morphology of muscle proprioceptors in the rat BE ACCEPTED IN PARTIAL FULFILLMENT OF THE REQUIREMNTS FOR THE DEGREE OF Master of Science

Larry J. Ream
Director of Graduate Programs in
Neuroscience and Physiology

Timothy C. Cope
Chair, Department of NCBP
Committee on

Final Examination

Timothy C. Cope, PhD
Chair, Department of NCBP

Larry J. Ream
Director of Graduate Studies in N & P

Robert E. W. Fyffe PhD
Vice President for Research and
Dean of the Graduate School

ABSTRACT

Gabriel, Hanna Marie. M.S. Department of Neuroscience, Cell Biology, & Physiology, Wright State University, 2015. Correlations Between Sensory Encoding and Central Morphology of Muscle Proprioceptors in the Rat

Until now, observations regarding the central morphology and organization of Ia, group II and Ib Golgi tendon organ afferents have been confined to the cat model. As the use of rodents in the study of the development and organization of segmental spinal cord circuitry increases, a complete account of the peripheral encoding and central connectivity of rodent muscle proprioceptors is necessary. The data presented in this study establish the central morphology and spatial distribution of 12 (4 of each class) functionally phenotyped muscle proprioceptor afferents in the rat by intracellular labeling with Neurobiotin. Each afferent type showed a characteristic central morphology and trajectory that was consistent with observations in the cat. However, variability between the two mammalian models was observed in the average distribution of synaptic contacts within each target lamina. Overall, our data suggests that the findings previously established in the cat are generalizable to other mammalian species.

TABLE OF CONTENTS

TABLE OF CONTENTS (continued)

LIST OF FIGURES

LIST OF TABLES

I. INTRODUCTION

Somatosensory feedback from muscle proprioceptors is essential to the spinal control of locomotion. Direct anatomical evidence of muscle proprioceptor central connections in correlation with the sensory signal encoded by peripheral receptors is essential to understanding the influence of somatosensory feedback on motor behavior (Dessem *et al.*, 1997; Arber, 2012; Zampieri *et al.*, 2014). Recently, molecular signaling processes contributing to the developmental organization of the neuronal circuits involved in motor control have being characterized using rodent models (Arber *et al.*, 2000; Inoue *et al.*, 2002; Patel *et al.*, 2003; Yoshida *et al.*, 2006). These studies have placed emphasis on the precise targeting of sensory axons (proprioceptive and cutaneous) in correlation with the positioning of motor pools to define factors that regulate circuit formation and axonal guidance during development. However, these rodent studies fail to differentiate between sensory signals generated by muscle spindles and Golgi tendon organs (GTOs), and instead, rely heavily on the central axonal trajectories and terminals zones of Ia, group II and Ib afferents, known only in the cat.

The peripheral structure and encoding of cat muscle proprioceptors have been extensively studied using anatomical and electrophysiological techniques (Boyd & Ward, 1975; Banks *et al.*, 1982). Based on these analysis muscle proprioceptors can be further distinguished as muscle spindles receiving Ia and group II sensory innervation, and Golgi tendon organ receiving Ib sensory innervation (Matthews, 1972). Centrally, electrophysiological measurements of extracellular potentials and intracellular recordings from localized neurons sub-serving motor control circuitry provide indirect evidence for

the functional connectivity of cat muscle proprioceptors. These observations are supported by direct evidence from intracellular labeling techniques characterizing the trajectory and axonal terminations of Ia, group II, and Ib muscle proprioceptors (Brown & Fyffe, 1978; Hongo *et al.*, 1978; Brown & Fyffe, 1979; Fyffe, 1979; Ishizuka *et al.*, 1979; Conradi *et al.*, 1983; Hoheisel *et al.*, 1989; Burke & Glenn, 1996). However, the number of intracellular labeling studies is limited especially for group II muscle spindle afferents (Fyffe, 1979; Hoheisel *et al.*, 1989).

With the transition to studying the neuronal organization of the segmental spinal circuits underlying motor control in the rodent, the peripheral structure and encoding properties of muscle proprioceptors has been revisited (Lewin & McMahon, 1991; De-Doncker *et al.*, 2003; Haftel *et al.*, 2004; Bullinger *et al.*, 2011) Qualitatively, rodent muscle proprioceptors are similar to the cat and can be further classified into Ia and group II muscle spindle afferents and Ib GTOs. However, unlike the cat, this analysis relies heavily on firing properties rather than conduction velocity (De-Doncker *et al.*, 2003) The central connectivity of these muscle proprioceptors has also been revisited using electrophysiological techniques (Haftel *et al.*, 2005; Bichler *et al.*, 2007). With the exception of a few studies that follow changes in Ia muscle spindle afferent projection after nerve injury (Alvarez *et al.*, 2011; Rotterman *et al.*, 2014), the axonal trajectory and connectivity of rodent muscle proprioceptors has not been established.

The purpose of this study was to characterize the central projections of rat muscle proprioceptors in direct correlation with their differential sensory encoding. Using an in vivo rodent model, muscle proprioceptor firing responses to muscle stretch were recorded intra-axonally within dorsal roots. Muscle proprioceptors were classified as Ia, group II,

or Ib afferents based on firing responses. In select cases classified afferents were intracellularly labeled, allowing for the analysis of central connectivity. In this study we demonstrate, for the first time in the rat, the functional connectivity of physiologically identified muscle proprioceptor afferents.

II. METHODS

Animals

All procedures and experiments were approved by the Wright State University Institutional Animal Care and Use Committee. Thirty (actual total number) adult female Wistar rats (250-300g, Charles Rivers Laboratory Wilmington, Va) were studied once each in single terminal experiments. All animals were housed in Wright State's Laboratory Animal Resources facility. Rats were kept in cages with food and water available *ad libitum.* Following terminal experiments, animals were overdosed with isoflurane anesthesia and their hearts surgically removed.

Terminal Experiments

Anesthesia and Vital Signs

Rats were deeply anesthetized (complete absence of withdrawal reflex) by inhalation of isoflurane, initially in an induction chamber (5% in 100% O_2) and for the remainder of the experiment via a tracheal cannula (1.5-2.5% in 100% O_2). Surgical and recording preparation followed by data collection lasted up to 15 hours. Subcutaneous injections of lactated ringer solution were given to support fluid levels and blood pressure. The rats' respiratory rate, pCO_2, and core temperature were monitored continuously; pulse rate and pO_2 were monitored intermittently. Variations in vital signs

that were sustained or that exceeded normal ranges (Muir *et al.*, 2000) were corrected by adjusting anesthesia (within the bounds of suppressing withdrawal reflex) and temperature was maintained (36-38ºC) by adjusting heat sources (heated water pad and radiant heat).

Surgical Dissection

Standard surgical procedures were applied as described in earlier reports from this laboratory, e.g. Bullinger *et al*., 2011. Briefly, ankle extensor muscles and nerves were uncovered dorsally by skin incision in the left leg, and lumbar dorsal roots 4-6 were exposed by skin incision, muscle dissection, and laminectomy. Rats were clamped at the snout and lumbar vertebral bodies 1-4 in a rigid recording frame; the left leg was clamped at the distal femur and tibia bones holding the knee joint at an angle of approximately 110-120º. The Achilles tendon of insertion common to the triceps surae muscles (lateral and medial gastrocnemii and soleus) was marked for its position to identify the muscle groups' resting length (Lr) with the ankle held at 90º. The Achilles tendon was then severed at the calcaneus and attached to a force and length-sensing servomotor (Model 305B-LR, Aurora Scientific Inc.) Triceps surae nerves were freed from the surrounding tissue and placed on a unipolar stimulating electrode; all other hindlimb nerves including common peroneal, sural, and posterior tibial nerves were crushed. Exposed tissues were covered with warm mineral oil in pools formed by attaching the edges of severed skin to the recording frame.

Electromechanical Study of Muscle Proprioceptors

Dorsal rootlets were carefully freed in continuity from overlying connective tissue and supported on bipolar hook electrodes within a millimeter or two from their entry into the dorsal spinal cord. Rootlets were selected for intra-axonal sampling when they produced orthodromic action potentials recorded extracellularly by the hook electrodes in response to electrical stimulation of triceps surae nerves or to stretch of triceps surae muscles. Glass micropipettes (ca. 15 MΩ filled with 2 M K^+ Acetate) were advanced in 1μm steps into the dorsal rootlet in order to penetrate axons and isolate their action potential firing. Randomly sampled axons of primary afferents were selected for study when electrical stimulation of triceps nerves in the periphery produced orthodromic action potentials that were readily resolvable and had conduction delay of <3 ms. Intra-axonal records of action potentials together with records of muscle length and force were digitized (20 kHz) and were monitored on-line and stored on computer for later analysis both using Spike2 software.

The firing of individual axons was examined in response to a battery of tests involving triceps surae contraction or passive stretch. These tests were designed to classify afferent axons into different types of muscle proprioceptors (Mathews 1972; see also Bullinger *et al.*, 2011) and to characterize how their firing encoded muscle length changes. Electrical stimulation of triceps surae nerves produced orthodromic action potentials from which we measured the axon's orthodromic conduction delay. This stimulation also evoked muscle twitches, and during the rise in force, afferents which paused were designated muscle spindle afferents, while those that accelerated firing were labeled tendon organs. Muscle spindle afferents were distinguished by their responses to

1 sec bouts of high frequency sinusoidal stretch, i.e. muscle vibration (100-333 Hz, 80μm): afferents that fired with nearly perfect entrainment to every sinusoid were designated group IA and those which fired with poor fidelity were called group II. One further distinction assigned to muscle spindle afferents was the presence of initial burst firing at the onset of ramp stretches (20 mm/s) for group IA but not for group II.

Further characterization of afferent encoding was based on firing in response to different forms of muscle stretch, including ramp-hold-release (1-3 mm; 4-20 mm/s ramp, 1 sec hold) stretch repeated every 4secs and three successive triangular stretches (4mm/s, 3mm) presented with the muscle held at fixed length and not contracting for >2min. Firing rates and change in rates occurring in different phases of these muscle stretches characterized encoding by muscle proprioceptors as defined in Results. Stretches were applied to the triceps surae group of muscles at each of three initial muscle lengths beginning with L_r. In all experiments we noted that when the Achilles tendon approximated L_r, passive tension was 10g ± 0.5g, and that stretching the muscle by an additional 1 or 2 mm each incremented passive tension by 10 g. Because there was greater precision in measuring force through the transducer than was measuring Lr by visual inspection of the position marker on the tendon, we used force to estimate and set muscle length at three different positions: 10g = Lr, 20g = Lr+1mm; 30g = Lr+2mm.

Intra-axonal Labeling

Twelve afferents physiologically classified as group Ia, II or Ib proprioceptors (4 each) as described above, were intracellularly injected through the recording pipette with 10% Neurobiotin (Vector Laboratories, Burlingame, CA, USA) in Tris Buffer (0.1 M Tris-OH, 1M Potassium Acetate, pH 7.6). Intra-axonal injection of Neurobiotin was

performed ~1 mm from the dorsal root entry zone. Positive current pulses were utilized to aid Neurobiotin passage into the fiber (5-15 nA delivered by 400-ms-long pulses at 2 Hz for 10-30 min). Injections lasting for >12 minutes and at membrane potential >-45 mV provided the best labeling of the axon's intra-spinal projections and collaterals. After label injection, the electrode was retracted and a minimum 6-h waiting period was allowed for anterograde labeling of central collaterals inside the spinal cord. Deeply anesthetized animals were then sacrificed by an intraperitoneal overdose of Euthasol (50mg/mL). Animals were transcardially perfused with ice-cold vascular rinse (0.01 M phosphate buffer with 0.8% NaCl, 0.025% KCl and 0.05% $NaHCO_3$, pH 7.4) followed by room temperature fixative (4% paraformaldehyde in 0.1 M phosphate buffer, pH 7.4). The lumbar spinal cord was quickly dissected and postfixed overnight in the same fixative at 4°C. The following day, spinal tissue was transferred to 0.01 M PBS and processed for *post hoc* immunohistochemistry as described below.

Anatomy

Immunohistochemistry

Transverse or sagittal sections (75 μm thick) of lower lumbar spinal cord were cut on a vibrating microtome, and collected in 0.01 M phosphate buffer with 0.9% NaCl (PBS, pH 7.4) for free floating immunohistochemistry. Nine afferents (3 of each class) were cut in the transverse plane, while 3 (1 of each class) were cut parasagitally.

Tissue sections were first blocked with 5% normal horse serum diluted 1:10 in phosphate-buffered saline (PBS) with 0.1% Triton X-100 (PBS-TX) for 30-60 min. Neurobiotin was revealed by incubating the sections for 2-3 h at room temperature in a

1:100 dilution (0.1M PBS-TX) of streptavidin conjugated to 488 nm (Life Technologies). Sections containing labeled axon collaterals were subsequently incubated overnight at 4°C with the following primary antibodies: anti-VGLUT1 (vesicular glutamate transporter; Synaptic Systems, Goettingen, Germany; Guinea Pig, 1:2000 dilution in PBS-TX 0.1%, pH 7.4) and anti-Neun (neuronal nuclear protein; Chemicon, Temecula, CA, USA; mouse, 1:1000 dilution in PBS-TX 0.1%, pH 7.4). The specificity and sensitivity of the primary antibodies in this study have been amply characterized for their specific labeling patterns in the spinal cord (Alvarez *et al.*, 2011; Rotterman *et al.*, 2014). Following overnight incubation, the sections were washed in PBS and immunoreactive sites were revealed with species-specific secondary antibodies raised in donkey and conjugated to Cy3 or Cy5 (Jackson Immunoresearch, West Grove, PA, USA) diluted 1:50 in PBS-TX 0.1%, pH 7.4. After 2-3 h incubation period in secondary antibodies, the sections were thoroughly washed in PBS, mounted on gelatin-coated slides, and coverslipped with Vectashield (Vector Labs, Burlingame, CA).

Confocal Microscopy and Quantitative Analysis

Images were obtained on a Fluoview 1000 Olympus (Center Valley, PA, USA) confocal microscope with a x10 objective at 1.0 μm Z-steps, x20 objective at .65 μm Z-steps, and x60 oil immersion objective at 0.5 μm Z-steps at 1.0 - 3.0 digital zoom. Sections were excited sequentially with the Streptavidin-488 nm (argon) laser, NeuN Cy3 (krypton, 568 nm) laser, and VGLUT1 Cy5 (HeNe, 633 nm) laser. All sections containing filled collaterals of sensory afferents were imaged. Fluoview software (Olympus) was utilized to analyze axon collateral trajectory and quantify Neurobiotin-filled boutons containing immunoreactivity for VGLUT1. Immunoreactivity is

considered positive for a given antigen if the fluorescence intensity is at least a twofold increase over background. Sections not meeting this criterion were discarded from examination, including ones exhibiting poor penetration of labeling into the middle of the tissue section.

Image stacks were quantitatively analyzed for immunofluorescence of Neurobiotin-filled structures including axons and varicosities (*en passant* and *terminal*) provisionally identified as synaptic boutons. Morphologically identified synaptic boutons were examined for co-localization with the vesicular glutamate transporter (VGLUT1) (Alvarez *et al*., 2011). Bouton distribution and density throughout each lamina or terminal zone was determined by the average number of synaptic contacts present in each lamina per 75 μm transverse section analyzed. The rostral caudal extent of staining, and therefore the total number of sections containing filled afferent collaterals, varied for each experiment. Therefore, the average number of boutons per 75 μm section was normalized to each individual afferent. Images were always analyzed in original, unprocessed form.

Figure Composition

Microscopic images were prepared by adjusting brightness and contrast in ImagePro Plus software (Media Cybernetics, Silver Springs, MD, USA) and always preserve all the information content of the images. Some images were sharpened with the use of a high-gauss filter in Image Pro. All figures were composed using CorelDRAW and/or Corel PHOTO-PAINT (Version x5)

III. RESULTS

In the present study a total of twelve (4 Ia, 4 group II, and 4 Ib Golgi tendon organ) afferents from triceps surae were physiologically characterized and intracellularly labeled with Neurobiotin. Systematic stretch paradigms were performed (refer to methods) to differentiate between each afferent class before labeling. Intra-axonal injections lasting >12 min, with stable membrane potential, produced the best labeling of central collaterals and the most extensive rostral-caudal staining. Spinal cord sections containing filled afferent collaterals were collected and analyzed, while tissue depths showing decreased immunofluorescence were discarded. Each physiologically characterized afferent was then analyzed to determine its central morphology and the distribution of synaptic boutons throughout each target lamina (IV-VI, VII, and LIX).

Afferent Central Trajectory

The main morphological features and physiological phenotype of each afferent type (Ia, Group II, and Ib) from triceps surae are shown in Figures 1-3, respectively. The individual afferents depicted in these figures were chosen as representative of the *typical* morphology and trajectory observed in the transverse plane for each afferent class studied. Each afferent class displayed a characteristic central morphology and trajectory after entering the spinal gray matter through the dorsal or medial border of the dorsal horn. Moreover, there was consistency in both the gross morphology and terminal branching patterns of each collateral within a given afferent class. These similarities were

observed not only within a single subject (rat), but also across collaterals in different subjects.

When viewed from serial sagittal sections (Fig 4), collaterals descended with a rostral tilt from their point of origin through the dorsal horn to their most distal projections in the intermediate / ventral gray matter. Therefore, within a single collateral, terminal aborizations in lamina V/VI are caudal to those in lamina VII or IX. This craniad tilt was most evident in Ia and group II afferents, though Ib afferents still showed a slight rostral tilt. Group II and Ib afferent collaterals occupy an isolated volume of spinal cord, with no overlap of the terminal arborizations of adjacent collaterals. In contrast, Ia collaterals exhibited overlap between terminal arborizations in lamina IX.

Ia Afferent Trajectory

After entering the dorsal gray matter, Ia afferent collaterals travel ventrally to the border of lamina V and VI before subdividing (some collaterals may give off simple branches at the level of lamina IV and V) and produced complex terminal arborizations in lamina VI. Collaterals then moved ventrally through lamina VII, toward the motor cell columns in lamina IX. Ia collaterals displayed variability in their advancement through lamina VII and into lamina IX (Fig. 1F). The majority of Ia collaterals penetrated to the level of the central canal and continued ventrolaterally at a 45˚ angle towards the triceps surae motor pool (dorsal half of lamina IX; (Nicolopoulos-Stournaras & Iles, 1983; Molander *et al.*, 1984; Swett *et al.*, 1986). In the second most common approach, collaterals traveled past the central canal to the ventral half of lamina VII before crossing into lamina IX. The divergent trajectory of collaterals advancing to lamina IX accounts

for a diffuse distribution of synaptic contacts, within lamina VII, along the lamina IX border (Fig. 1E). The least common approach into the motor nuclei was achieved by projecting through the most dorsolateral aspect of laminal VII (dorsal medial to the motor nuclei) and crossing into the most dorsal aspect of lamina IX, before bifurcating and traveling directly ventral to arborize in central lamina IX.

The density and distribution of Ia synaptic contacts in each lamina is directly related to their gross morphology. Each Ia afferent distributed terminal arborizations to three main zones: (1) the medial two thirds of lamina VI (the intermediate region); (2) the dorsal lateral aspect of lamina VII (the Ia inhibitory interneuron region); and (3) lamina IX (the motor nuclei) (Fig. 1E). Terminal arborizations in lamina VI were the most complex out of the three terminal zones. Collaterals reaching the lateral third of lamina VI were less developed and occurred sparsely in comparison to the complex arborizations that frequently arise in the medial two thirds of the lamina. Ia collateral branching in lamina VII was the simplest of all the lamina, and consistently provided the least amount of synaptic contacts (Table 1). The highest bouton density in lamina VII was usually located in the dorsal part of lamina VII and along the dorsal half of the lamina IX border. Variability in the ventrolateral approach of collaterals through lamina VII to reach lamina IX likely accounts for the wide distribution of the bouton terminal zone along the lamina IX border. Lamina IX arborizations were intermediate in their level of complexity in their branching pattern. Ia afferent collaterals showed a wide distribution of contacts throughout the entirety of lamina IX. However, the highest density of contacts resided in the dorsal half of the lamina.

Axosomatic and axodendritic contacts, identified by Neurobiotin filled varicosities colocalized with VGLUT1 immunoreactivity, were seen on small/medium sized neurons in lamina V/VI, medium and spindle shaped neurons in lamina VII, and large neurons in lamina IX (Fig. 1.VI, VII, LIX). Neurons measuring ≥30 μM were characterized as motor neurons. Axosomatic contacts were most commonly observed in the dorsal portion of lamina IX, closer to the homonymous motor cell column for triceps surae, while contacts in the ventral half of lamina IX were primarily axodendritic.

Group II Afferent Trajectory

Group II afferent collaterals typically penetrated to the level of lamina V before subdividing and traveling through the medial two thirds of the dorsal horn into more ventral gray matter. Small branches with limited contacts were occasionally given off more dorsal in lamina IV. Collaterals then moved dorsolaterally through lamina VII and terminated in dorsal lamina IX (Fig. 2E). Continuations of collateral branches traveling ventral of lamina VI into lamina VII and IX were noticeably thinner than those in Ia afferents. This characteristic could be used as a distinguishing factor between the two classes. Similar to the variability found in Ia afferents, some group II collaterals traveled ventral of the central canal in lamina VII before crossing into lamina IX, or took a dorsal lateral approach through lamina VII into the most dorsal aspect of lamina IX before bifurcating and traveling directly ventral to arborize in central lamina IX. The terminal zone in the dorsal two-thirds of lamina IX is another striking and distinguishing characteristic of group II afferents. Only one group II afferent in this study exhibited collaterals traveling to the more ventral portion of lamina IX.

Each group II afferent distributed terminal arborizations to three main zones: (1) the medial portion of lamina V and VI, mainly lamina VI; (2) the dorsolateral portion of LVII; and (3) the dorsal two-thirds of lamina IX (Fig. 2D). Group II afferent collaterals showed the greatest variability in the complexity of their terminal arborizations and number of synaptic contacts in each target lamina. Arborization patterns in lamina V/VI, VII, and LIX varied from highly developed and extensive, to weakly developed with simple branching. Therefore, the number of active synaptic contacts in each lamina was also highly variable.

Axosomatic and axodendritic contacts were observed on small and medium sized neurons in LV and LVI, on medium sized neurons in LVII, and on large neurons in LIX . The distribution of axonal contacts in lamina IX were consistently localized in the dorsal portion of the lamina, closer to the homonymous motor cell column for triceps surae (Nicolopoulos-Stournaras & Iles, 1983; Swett *et al.*, 1986). There were only a few occasions where group II collaterals made axosomatic or axodendritic contacts in the ventral portion of lamina LIX. (Fig. 2.VI, VII, LIX)

Ib Golgi Tendon Organ Afferent Trajectory

Ib Golgi tendon organ afferents traveled ventrally to the border of lamina IV and V or lamina V before subdividing. Collaterals entering lamina V and VI, mostly VI, would often ramify into complex, wide triangular patterns. These “fan-shaped” arborizations usually situated the terminal zone for these collaterals in the medial to central portion of lamina VI and extended to the dorsal aspect of lamina VII (Fig. 3E). Collateral branching rarely reached the lateral portion of lamina VI. However, complex

arborizations in the medial part of lamina VI would occasionally extend a single branch into this area. Projections into lamina VII were primarily located dorsal of the central canal along the lamina VI/VII border. However, some collaterals would occasionally extend a single branch containing 1-6 synaptic boutons to the level of the central canal. The most distinguishing characteristic of Ib afferent collaterals, in comparison to Ia and Group II, was the absence of projections to the motor nuclei.

Ib afferent terminations were primarily located in (1) the dorsal and central parts of lamina VI; and (2) the dorsal aspect of lamina VII along the lamina VI/VII border (Fig. 3D). Arborizations in lamina V and VI were often very complex—exhibiting a characteristic fan-shape, which extended into the dorsal aspect of lamina VII. Axosomatic and axodendritic contacts, identified by the colocalization of filled afferent boutons with VGlut1, were seen on small/medium sized neurons in lamina V/VI, and medium or spindle shaped neurons in the dorsal parts of lamina VII. However, collateral branches extending to the level of central lamina VII never resulted in an axosomatic contact.

Density and Distribution of Boutons Within Target Lamiae

Bouton distribution and density throughout each lamina or terminal zone was determined by the average number of synaptic contacts present in each lamina per 75 μM transverse section analyzed. These data are presented in Table 1. Synaptic varicosities (*en passant* and *terminal*) were identified morphologically and further verified by the expression of vesicular glutamate transporter (VGLUT1) within each Neurobiotin filled synaptic bouton (Alvarez *et al.,* 2011; Rotterman *et al.,* 2014). Variability in the location

and distribution of synaptic contacts throughout each target lamina was observed between and within each afferent class: Ia, group II, and Ib GTO. This variability was reflective of the characteristic branching patterns and terminal zones of each afferent class.

All Neurobiotin labeled Ia afferent collateral boutons in this study contained immunoreactivity for the synaptic protein VGLUT1. In contrast, Neurobiotin filled varicosities in both group II and Ib GTO afferent collaterals (afferent 5 through 9) showed inconsistent immunoreactivity for VGLUT1 throughout individual 75 μM sections and in each target lamina. We suspect some technical or methodological explanation for the lack of VGLUT1 content in these synaptic boutons. This observation could be the result of poor antibody penetration, however we cannot rule out the possibility that Group II and Ib synapses express an alternative complement of synaptic proteins.

Table 2 illustrates the population of Neurobiotin-filled group II and Ib afferent collateral boutons that contained immunoreactivity for the synaptic protein VGLUT1. It should be noted that, within a single afferent, the average number of boutons in each lamina verified by VGLUT1 was sometimes comparable to the *total* number of synaptic contacts in each lamina. However, on some occasions, the average number of contacts verified by VGLUT1 were greatly outnumbered by those synaptic boutons not expressing the vesicular transporter.

Variability

Each Ia afferent in this study showed a comparable number of contacts in lamina VII and LIX, however some variability was evident in lamina IV-VI (Table 1). Afferents

2 & 3 showed the highest number of synaptic contacts in lamina IX (21.47 ± 27.93; 19.98 ± 22.87), an intermediate amount in lamina IV-VI (8.71 ± 12.23; 12.79 ± 19.64) and the lowest number of contacts in lamina VII (4.85 ± 7.64; 7.33 ± 11.29). Afferent 1 followed a comparable distribution pattern in lamina VII (5.83 ± 11.48) and IX (19.95 ± 26.18), however the average number of contacts in lamina IV-VI (23.81 ± 42.64) was noticeably higher than afferents 2 and 3. Physiological analysis revealed that afferents 2 and 3 displayed higher peak dynamic firing rates (afferent 2: 248.76 pps, afferent 3: 238.1 pps) compared to afferent 1 (166.67 pps).

Only one group II afferent (afferent 4) consistently expressed VGLUT1 immunoreactivity in its Neurobiotin-filled boutons like the Ia afferents (Table 1). It is worth noting that this afferent, unlike afferents 5 & 6, also displayed a comparable average number of synaptic contacts in lamina IX (25 ± 37.36) to the Ia afferents. When analyzed physiologically, afferent 4 displayed high dynamic sensitivity achieving similar peak dynamic firing rates (157.23) to Ia afferents. However, despite its Ia-like dynamic sensitivity, afferent 4 showed less adaptation during transition from dynamic to static muscle stretch (low dynamic index value), and continued to fire on the release from muscle stretch similar to other group II afferents.

IV. DISCUSSION

The present study demonstrates, for the first time in adult rodents, the central trajectory, terminal distributions, and peripheral encoding of muscle proprioceptors. The information presented provides valuable insight on the central integration of sensory input and a comprehensive understanding of the organization and functional contribution of muscle proprioceptors in spinal sensorimotor circuits. Until now, observations regarding the central morphology and organization of Ia, group II and Ib afferents have been confined to the cat model. As the use of rodents in the study of sensorimotor circuitry and development increases, a complete account of the peripheral encoding and central connectivity of rodent muscle proprioceptors is necessary before important conclusions are drawn in the absence of direct information. Our data provides insight for the manner in which proprioceptive feedback influences these rodent spinal circuits, while also expanding our overall understanding of this progressing mammalian model.

Overall, our data suggests that the findings previously only available in the cat are generalizable to other mammalian species. In agreement with previous studies in the cat (Brown & Fyffe, 1978; Hongo *et al.*, 1978; Brown & Fyffe, 1979; Fyffe, 1979; Ishizuka *et al.*, 1979; Brown, 1981; Conradi *et al.*, 1983; Fyffe, 1984; Burke & Glenn, 1996), we found consistency in both the gross morphology and terminal branching patterns of each collateral within a given afferent class. By means of intra-axonal staining with

Neurobiotin, we were able to provide direct and detailed information regarding the central trajectory and peripheral encoding of Ia, group II and Ib GTO afferents. Comparable to the cat, Ia and group II afferents shared a similar ventral trajectory through the spinal gray matter, producing terminal arborizations in lamina V/VI, lamina VII, and lamina IX, while Ib afferents displayed the distinguishing characteristic of only projecting to lamina V/VI and lamina VII. Similar to the cat, variability in the location and distribution of synaptic contacts throughout each target lamina was observed between and within each afferent class (Ia, group II and Ib GTO). It was within these unique terminal fields that we observed differences between the central morphology of rat and cat muscle proprioceptor afferents.

It is of interest to determine potential relationships between the terminal zones of afferent collaterals within respective target laminae and the physiological phenotypes of Ia, group II and Ib muscle proprioceptors. The terminal distribution areas of Ia and Ib afferents from cat triceps surae are well established (Brown & Fyffe, 1978; Hongo *et al.*, 1978; Brown & Fyffe, 1979; Fyffe, 1979; Ishizuka *et al.*, 1979; Brown, 1981; Conradi *et al.*, 1983; Fyffe, 1984; Burke & Glenn, 1996). However, information regarding the trajectory and morphology of group II afferents in the cat is limited to two studies (Fyffe, 1979; Hoheisel *et al.*, 1989). A diagrammatic representation of the average extents (areas of termination) of Ia, group II, and Ib afferents from lateral gastrocnemius/soleus in the cat and triceps surae in the rat (Fig. 5) provides an interesting comparison between the two models.

on average, Ib afferents have the simplest termination pattern, limited to a single area including lamina V, VI and dorsal lamina VII. In contrast, Ia and group II collaterals

generate 3 separate terminal zones. Ia collaterals primarily terminate in (1) medial lamina VI, (2) in lamina VII dorsal and dorso-medial to lamina IX (3) and within lamina IX, while group II collaterals take a lateral path through the dorsal horn, terminating in (1) lamina IV-VI, (2) lamina VII, and (3) in the homonymous motor cell column in lamina IX (Romanes, 1951). Figure 5 illustrates the differences in the average extents (terminal fields) of terminal arborizations observed between the rat and cat model. The average terminal zones of Ib afferents (Fig. 5E & F) appear to be consistent between the rat and cat, while both Ia (Fig. 5A & B) and group II (Fig. 5C & D) afferent collaterals displayed striking differences in their termination patterns.

The terminal fields of Ia afferent collaterals in the rat differ from the cat in two noticeable ways: (1) rats have a larger terminal field localized in the medial two-thirds of the lamina VI, and (2) rats have a larger average terminal field covering the entirety of lamina IX. By contrast, Ia terminal arborizations in the cat are more restricted to medial lamina VI and dorsal lamina XI, though some collaterals in the cat may project to the ventral aspect of lamina IX (Brown & Fyffe, 1978; Ishizuka *et al.*, 1979; Brown, 1981; Fyffe, 1984; Burke & Glenn, 1996). Interestingly, Ia collaterals projecting into ventral lamina IX usually traverse the dorsolateral aspect of lamia VII (dorsal medial to the motor nuclei) and bifurcate in the dorsal portion of lamina IX before traveling directly to the ventral third of the lamina. A study by Ishuzuka *et al*., (1979) revealed that this pattern of trajectory was most common in cat soleus afferents. Interestingly, this unique, yet atypical, trajectory was also observed in both Ia and group II triceps surae afferents in the rat. In the cat, the average terminal field in lamina VII for Ia afferents collaterals is located in the dorsolateral aspect of the lamina. In contrast, the lamina VII terminal field

in the rodent has a larger dorso-ventral extent and is located along the lamina IX border. The divergent trajectory of collaterals advancing to lamina IX may account for the differences in the extent of afferent terminations within lamina VII and the larger terminal field throughout the entirety of lamina IX observed in the rat.

In the cat, group II afferents form terminal zones within the lateral aspect of the dorsal horn, while rodent group II afferents display a similar distribution pattern to Ia afferents and are localized medially throughout lamina IV-VI. The average extent of group II afferents in lamina VII and LIX are comparable between both animal models. The medial distribution of rat group II afferents in the dorsal horn, in combination with the more medial/central Ia terminal zone, creates a significant overlap between Ia, group II and Ib afferents in lamina VI. This observation is in contrast to the terminal field of group II collaterals in the cat, which show no overlap with Ia afferents in the intermediate region (Fig. 5G & H). This observation, along with the quantified distribution of synaptic contacts within each target laminae, provides further anatomical evidence supporting electrophysiological studies focused on the convergence of sensory information from each class of muscle proprioceptor afferents onto intermediate zone interneurons (Fetz *et al.*, 1979; Jankowska *et al.*, 1981a; Jankowska *et al.*, 1981b, c; Harrison & Jankowska, 1985; Jankowska & Edgley, 2010; Arber, 2012).

In conclusion, the data presented in this study establish the central morphology and spatial distribution of physiologically identified muscle proprioceptive afferents in the rodent. These anatomical data provide a basis/control reference for molecular signaling studies seeking to understand processes contributing to the developmental

organization of the segmental spinal cord and further insight into the precise patterns of sensory input/integration which influence locomotor output.

REFERENCES

Alvarez FJ, Titus-Mitchell HE, Bullinger KL, Kraszpulski M, Nardelli P & Cope TC. (2011). Permanent central synaptic disconnection of proprioceptors after nerve injury and regeneration. I. Loss of VGLUT1/IA synapses on motoneurons. *J Neurophysiol* **106,** 2450-2470.

Arber S. (2012). Motor circuits in action: specification, connectivity, and function. *Neuron* **74,** 975-989.

Arber S, Ladle DR, Lin JH, Frank E & Jessell TM. (2000). ETS gene Er81 controls the formation of functional connections between group Ia sensory afferents and motor neurons. *Cell* **101,** 485-498.

Banks RW, Barker D & Stacey MJ. (1982). Form and distribution of sensory terminals in cat hindlimb muscle spindles. *Philos Trans R Soc Lond B Biol Sci* **299,** 329-364.

Bichler EK, Nakanishi ST, Wang QB, Pinter MJ, Rich MM & Cope TC. (2007). Enhanced transmission at a spinal synapse triggered in vivo by an injury signal independent of altered synaptic activity. *J Neurosci* **27,** 12851-12859.

Boyd IA & Ward J. (1975). Motor control of nuclear bag and nuclear chain intrafusal fibres in isolated living muscle spindles from the cat. *J Physiol* **244,** 83-112.

Brown AG. (1981). *Organization in the Spinal Cord: The Anatomy and Physiology of Identified Neurons.* Springer-Verlag Berlin, Heidelberg, Great Britain.

Brown AG & Fyffe RE. (1978). The morphology of group Ia afferent fibre collaterals in the spinal cord of the cat. *J Physiol* **274,** 111-127.

Brown AG & Fyffe RE. (1979). The morphology of group Ib afferent fibre collaterals in the spinal cord of the cat. *J Physiol* **296,** 215-226.

Bullinger KL, Nardelli P, Wang Q, Rich MM & Cope TC. (2011). Oxaliplatin neurotoxicity of sensory transduction in rat proprioceptors. *J Neurophysiol* **106,** 704-709

Burke RE & Glenn LL. (1996). Horseradish peroxidase study of the spatial and electrotonic distribution of group Ia synapses on type-identified ankle extensor motoneurons in the cat. *J Comp Neurol* **372,** 465-485.

Conradi S, Cullheim S, Gollvik L & Kellerth JO. (1983). Electron microscopic observations on the synaptic contacts of group Ia muscle spindle afferents in the cat lumbosacral spinal cord. *Brain Res* **265,** 31-39.

De-Doncker L, Picquet F, Petit J & Falempin M. (2003). Characterization of spindle afferents in rat soleus muscle using ramp-and-hold and sinusoidal stretches. *J Neurophysiol* **89,** 442-449.

Dessem D, Donga R & Luo P. (1997). Primary- and secondary-like jaw-muscle spindle afferents have characteristic topographic distributions. *J Neurophysiol* **77,** 2925-2944.

Fetz EE, Jankowska E, Johannisson T & Lipski J. (1979). Autogenetic inhibition of motoneurones by impulses in group Ia muscle spindle afferents. *J Physiol* **293,** 173-195.

Fyffe REW. (1979). The morphology of Group II muscle afferent fibre collaterals *J Physiol* 39-40.

Fyffe REW. (1984). Afferent Fibers. In *Handbook of the Spinal Cord* David RA, ed. pp. 70-136. Marcel Dekker, Inc, New York, New York.

Haftel VK, Bichler EK, Nichols TR, Pinter MJ & Cope TC. (2004). Movement reduces the dynamic response of muscle spindle afferents and motoneuron synaptic potentials in rat. *J Neurophysiol* **91,** 2164-2171.

Haftel VK, Bichler EK, Wang QB, Prather JF, Pinter MJ & Cope TC. (2005). Central suppression of regenerated proprioceptive afferents. *J Neurosci* **25,** 4733-4742.

Harrison PJ & Jankowska E. (1985). Sources of input to interneurones mediating group I non-reciprocal inhibition of motoneurones in the cat. *J Physiol* **361,** 379-401.

Hoheisel U, Lehmann-Willenbrock E & Mense S. (1989). Termination patterns of identified group II and III afferent fibres from deep tissues in the spinal cord of the cat. *Neuroscience* **28,** 495-507.

Hongo T, Ishizuka N, Mannen H & Sasaki S. (1978). Axonal trajectory of single group Ia and Ib fibers in the cat spinal cord. *Neurosci Lett* **8,** 321-328.

Inoue K, Ozaki S, Shiga T, Ito K, Masuda T, Okado N, Iseda T, Kawaguchi S, Ogawa M, Bae SC, Yamashita N, Itohara S, Kudo N & Ito Y. (2002). Runx3 controls the axonal projection of proprioceptive dorsal root ganglion neurons. *Nat Neurosci* **5,** 946-954.

Ishizuka N, Mannen H, Hongo T & Sasaki S. (1979). Trajectory of group Ia afferent fibers stained with horseradish peroxidase in the lumbosacral spinal cord of the cat: three dimensional reconstructions from serial sections. *J Comp Neurol* **186,** 189-211.

Jankowska E & Edgley SA. (2010). Functional subdivision of feline spinal interneurons in reflex pathways from group Ib and II muscle afferents; an update. *Eur J Neurosci* **32,** 881-893.

Jankowska E, Johannisson T & Lipski J. (1981a). Common interneurones in reflex pathways from group 1a and 1b afferents of ankle extensors in the cat. *J Physiol* **310,** 381-402.

Jankowska E, McCrea D & Mackel R. (1981b). Oligosynaptic excitation of motoneurones by impulses in group Ia muscle spindle afferents in the cat. *J Physiol* **316,** 411-425.

Jankowska E, McCrea D & Mackel R. (1981c). Pattern of 'non-reciprocal' inhibition of motoneurones by impulses in group Ia muscle spindle afferents in the cat. *J Physiol* **316,** 393-409.

Lewin GR & McMahon SB. (1991). Physiological properties of primary sensory neurons appropriately and inappropriately innervating skin in the adult rat. *J Neurophysiol* **66,** 1205-1217.

Matthews P. (1972). *Mammalian Muscle Receptors and Their Central Actions*. The Williams and Wilkins Company, Baltimore.

Molander C, Xu Q & Grant G. (1984). The cytoarchitectonic organization of the spinal cord in the rat. I. The lower thoracic and lumbosacral cord. *J Comp Neurol* **230,** 133-141.

Muir, Hubbell, Skarda & Bednarski. (2000). *Veterinary Anesthesia*. Mosby Inc., St. Louis, Missouri.

Nicolopoulos-Stournaras S & Iles JF. (1983). Motor neuron columns in the lumbar spinal cord of the rat. *J Comp Neurol* **217,** 75-85.

Patel TD, Kramer I, Kucera J, Niederkofler V, Jessell TM, Arber S & Snider WD. (2003). Peripheral NT3 signaling is required for ETS protein expression and central patterning of proprioceptive sensory afferents. *Neuron* **38,** 403-416.

Romanes GJ. (1951). The motor cell columns of the lumbo-sacral spinal cord of the cat. *J Comp Neurol* **94,** 313-363.

Rotterman TM, Nardelli P, Cope TC & Alvarez FJ. (2014). Normal distribution of VGLUT1 synapses on spinal motoneuron dendrites and their reorganization after nerve injury. *J Neurosci* **34,** 3475-3492.

Swett JE, Wikholm RP, Blanks RH, Swett AL & Conley LC. (1986). Motoneurons of the rat sciatic nerve. *Exp Neurol* **93,** 227-252.

Yoshida Y, Han B, Mendelsohn M & Jessell TM. (2006). PlexinA1 signaling directs the segregation of proprioceptive sensory axons in the developing spinal cord. *Neuron* **52,** 775-788.

Zampieri N, Jessell TM & Murray AJ. (2014). Mapping sensory circuits by anterograde transsynaptic transfer of recombinant rabies virus. *Neuron* **81,** 766-778.

FIGURE 1

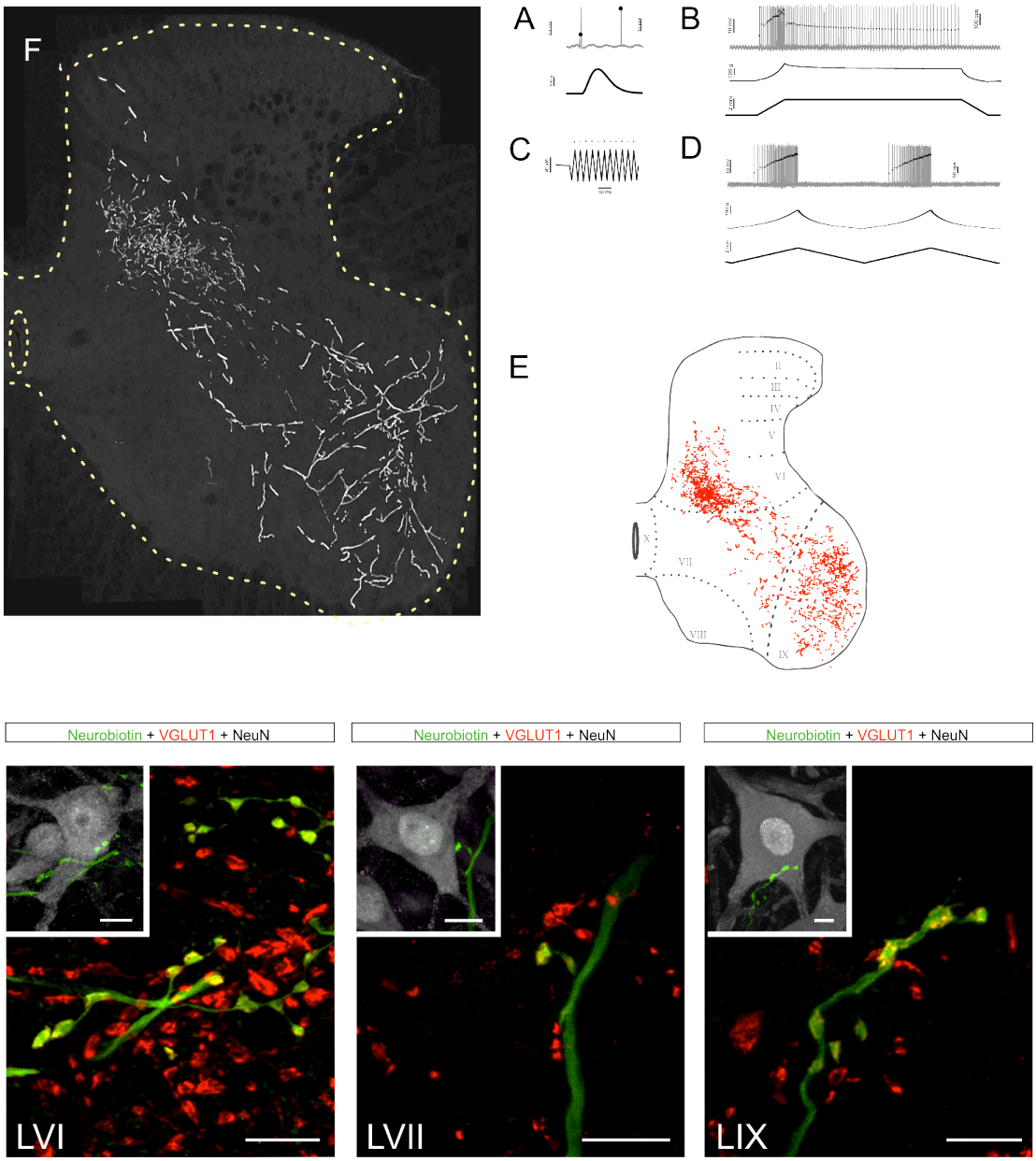
F
A
B
C
D
E
II
III
IV
V
VI
X
VII
VIII
IX
Neurobiotin + VGLUT1 + NeuN
Neurobiotin + VGLUT1 + NeuN
Neurobiotin + VGLUT1 + NeuN
LVI
LVII
LIX

Figure 1. Trajectories and VGLUT1 immunoreactivites of Ia afferent collaterals together with corresponding physiological phenotype of the depicted afferent. All anatomical and physiological data, with the exception of lamina contacs in LVI, LVII and LIX, are from the same afferent. A - D: Consistent with Ia afferent physiology, this afferent paused firing during the rising phase of isometric twitch contraction, displayed high frequency initial bursting at the onset of muscle stretch, and showed 1:1 firing entrainment to high frequency vibration (≥ 100Hz). F: Superimposed confocal images (20x) of sequential 75μM transverse sections (1.725 mM) within a single Ia afferent. Afferent was chosen based on success of staining and considered representative of the *typical* afferent trajectory observed for all Ia afferents (n=3) in this study. Afferent collaterals were imaged and a photomontage of each 75 μM section was constructed. Sequential sections were superimposed in relation to the borders of the gray matter and the central canal to create the illusion of "looking through" several tissue sections. Collaterals with branches in lamina V/VI, VII, and IX are easily observed. Spinal gray matter and central canal are outlined in dashed yellow line. E: Distribution of Neurobiotin-filled synaptic varicosities containing immunoreactivity for VGLUT1. Illustration is representative of terminals throughout the entire rostral-caudal extent of the same Ia afferent depicted in A-F. High magnification confocal microscopy of Neurobiotin-filled collaterals (green, 448 nm) within each target lamina (LVI, LVII, and LIX) containing immunoreactivity for VGLUT1 (red, cy3). Each collateral demonstrates an example of axosomatic and/or axodendritic (gray, NeuN) contacts found within each target lamina. Scale bars = 10 μM (images are at the same magnification).

FIGURE 2

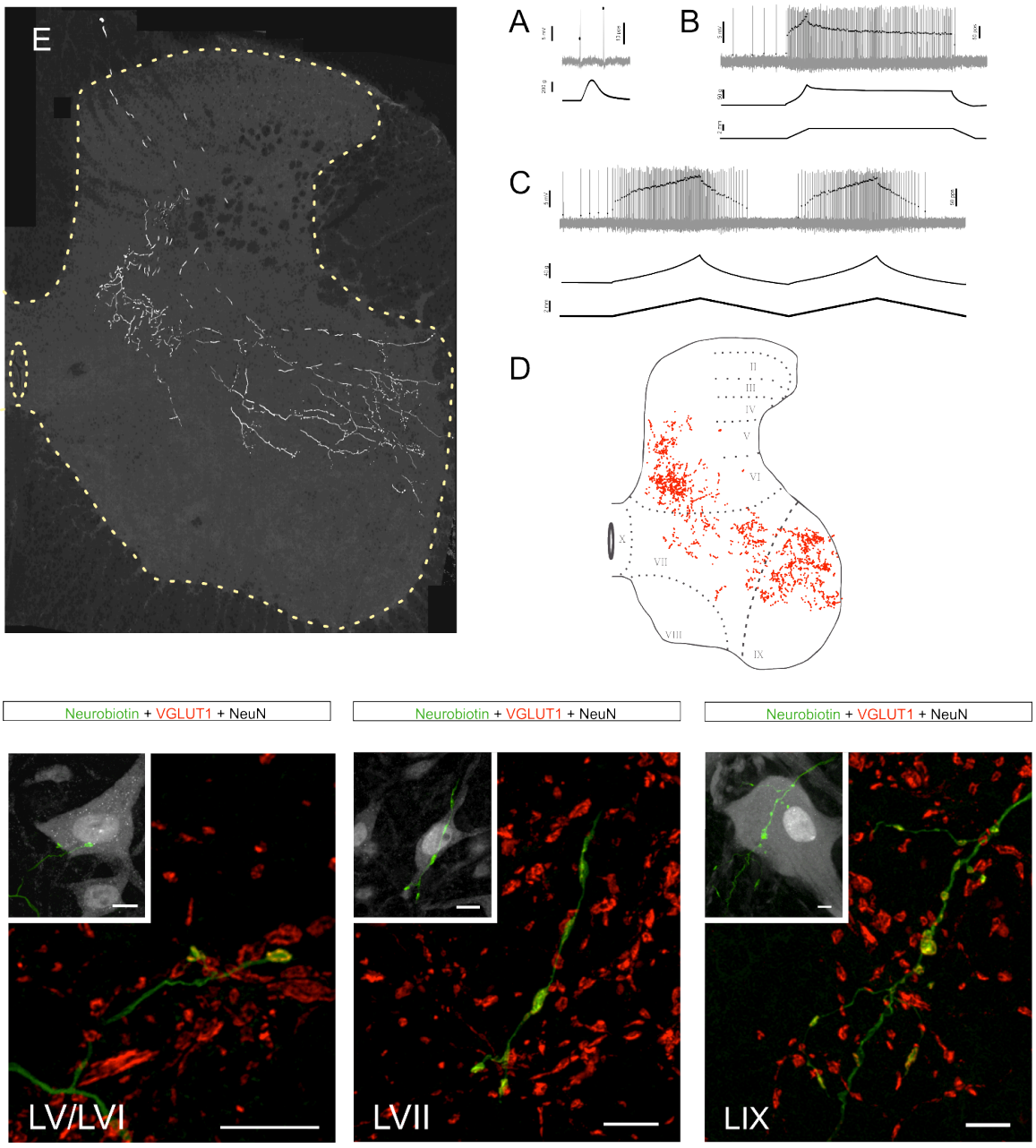
E
A
B
C
D
II
III
IV
V
VI
X
VII
VIII
IX
Neurobiotin + VGLUT1 + NeuN
Neurobiotin + VGLUT1 + NeuN
Neurobiotin + VGLUT1 + NeuN
LV/LVI
LVII
LIX

Figure 2. Trajectories and VGLUT1 immunoreactivites of group II afferent collaterals together with corresponding physiological phenotype of the depicted afferent. A- C: Consistent with group II afferent physiology, this afferent paused firing during the rising phase of isometric twitch contraction, failed to displayed high frequency initial bursting at the onset of muscle stretch, and did not show 1:1 firing entrainment to high frequency vibration (≥ 100Hz). All data presented in this figure are from the same group II afferent. E: Superimposed confocal images (20x) of sequential 75μM transverse sections (825 μM) within a single group II afferent. Afferent was chosen based on success of staining and considered representative of the *typical* afferent trajectory observed for all Group II afferents (n=3) in this study. Afferent collaterals were imaged and a photomontage of each 75 μM section was constructed. Sequential sections were superimposed in relation to the borders of the gray matter and the central canal to create the illusion of "looking through" several tissue sections. Collaterals with branches in lamina V/VI, VII, and IX are easily observed. Spinal gray matter and central canal are outlined in dashed yellow line. D: Distribution of Neurobiotin-filled synaptic varicosities containing immunoreactivity for VGLUT1. Illustration is representative of terminals throughout the entire rostral-caudal extent of the same group II afferent depicted in A-E. High magnification confocal microscopy of Neurobiotin-filled collaterals (green, 448 nm) within each target lamina (LV/VI, LVII, and LIX) containing immunoreactivity for VGLUT1 (red, cy3). Each collateral demonstrates an example of axosomatic and/or axodendritic (gray, NeuN) contacts found within each target lamina. Scale bars = 10 μM (images are at the same magnification).

FIGURE 3

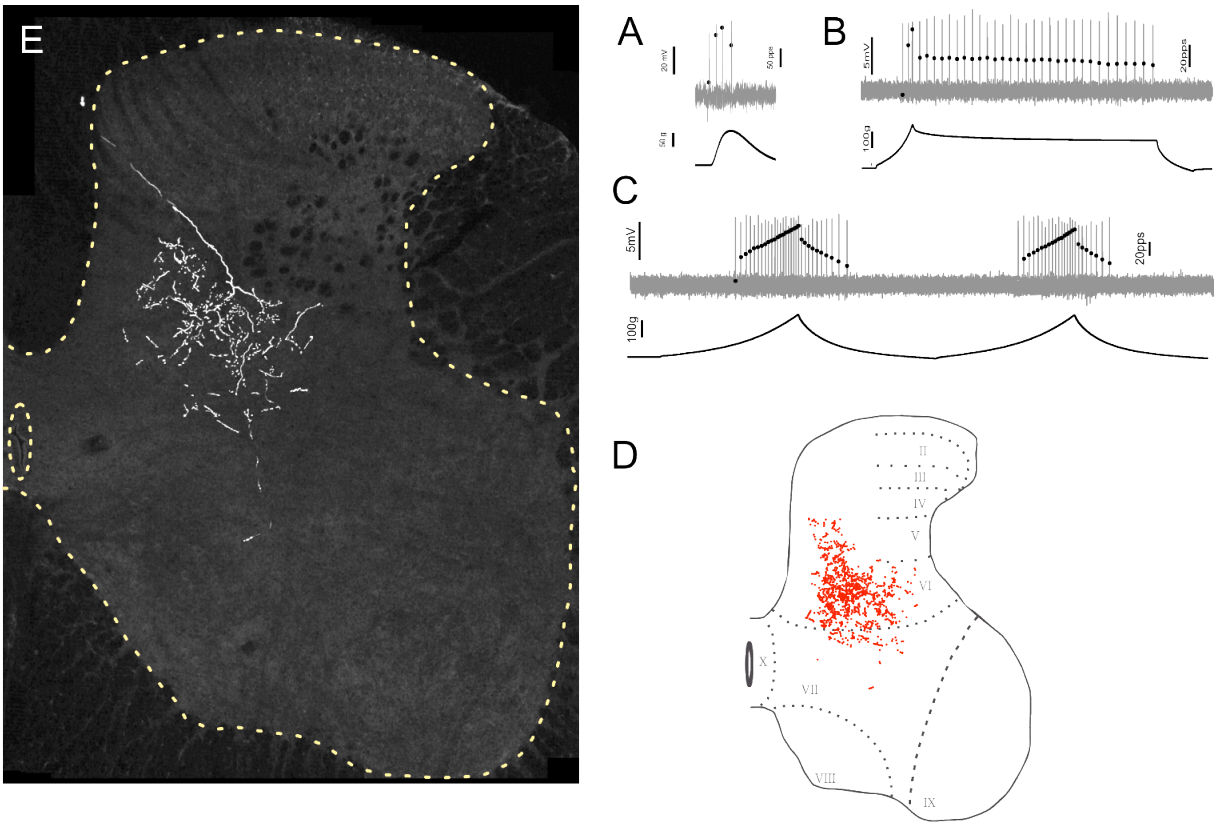
E
A
B
C
D
5mV
20pps
100g
II
III
IV
V
VI
X
VII
VIII
IX

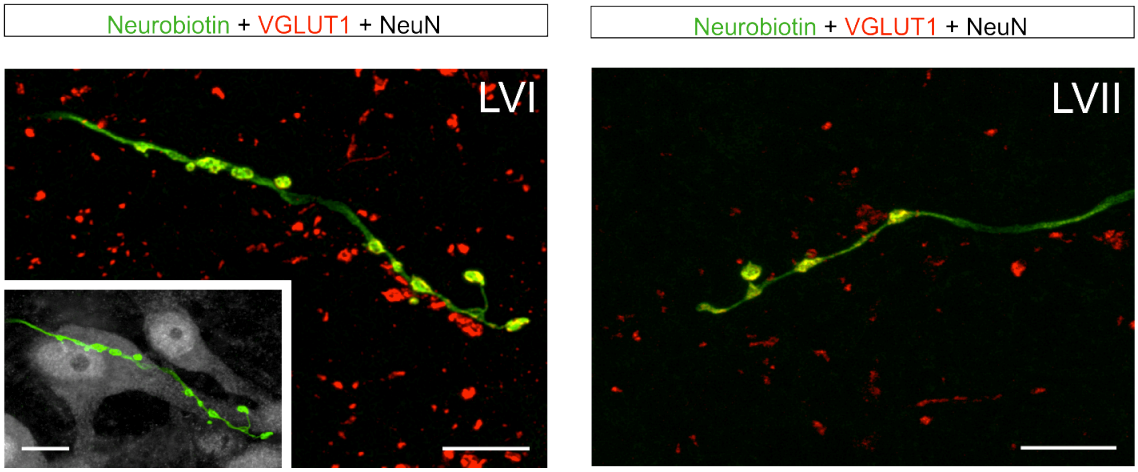
Neurobiotin + VGLUT1 + NeuN
LVI
Neurobiotin + VGLUT1 + NeuN
LVII

Figure 3. Trajectories and VGLUT1 immunoreactivites of Ib GTO afferent collaterals together with corresponding physiological phenotype. A- C: Consistent with Ib afferent physiology, this afferent accelerated firing during the rising phase of isometric twitch contraction, failed to displayed high frequency initial bursting at the onset of muscle stretch, and did not show 1:1 firing entrainment to high frequency vibration (≥ 100Hz). All data presented in this figure are from the same group II afferent. E: Superimposed confocal images (20x) of sequential 75μM transverse sections (825 μM) within a single group II afferent. Afferent was chosen based on success of staining and considered representative of the *typical* afferent trajectory observed for all Ib afferents (n=3) in this study. Afferent collaterals were imaged and a photomontage of each 75 μM section was constructed. Sequential sections were superimposed in relation to the borders of the gray matter and the central canal to create the illusion of "looking through" several tissue sections. Collaterals with branches in lamina V/VI and VII are easily observed. Spinal gray matter and central canal are outlined in dashed yellow line. D: Distribution of Neurobiotin-filled synaptic varicosities containing immunoreactivity for VGLUT1. Illustration is representative of terminals throughout the entire rostral-caudal extent of the same group II afferent depicted in A-E. High magnification confocal microscopy of Neurobiotin-filled collaterals (green, 448 nm) within each target lamina (LV/VI and LVII) containing immunoreactivity for VGLUT1 (red, cy3). Each collateral demonstrates an example of axosomatic and/or axodendritic (gray, NeuN) contacts found within each target lamina. No axosomatic contacts were found in the ventral aspect of LVII (depicted above). Scale bars = 10 μM (images are at the same magnification).

FIGURE 4

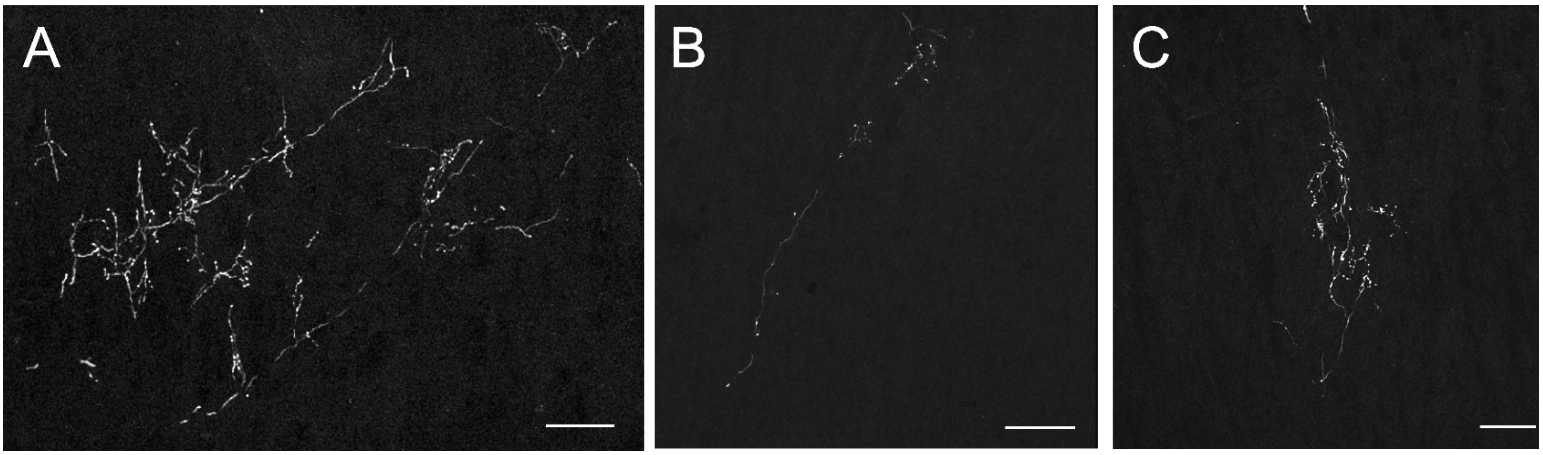

Figure 4. Low magnification confocal images from sagital sections of each afferent class innervating triceps surae: (A) Ia, (B) Group II, and (C) Ib GTO. A: Superimposed confocal images (10x) of sequential 75 μM sagital sections (150 μM) within a single Ia afferent. B,C: 75 μM sagital sections. Each collateral descended with a rostral tilt from their point of origin (very slight in Ib afferents) through the dorsal horn to their most distal projections in the intermediate / ventral gray matter. Therefore, within a single Ia or group II collateral, terminal aborizations in LV/VI are caudal to those in LVII or LIX. Group II and Ib afferent collaterals occupy an isolated volume of spinal cord, with no overlap of the terminal arborizations of adjacent collaterals, while Ia collaterals exhibited overlap between terminal arborizations in lamina IX. Scale bars = 100 μM (Images are at the same magnification)

FIGURE 5

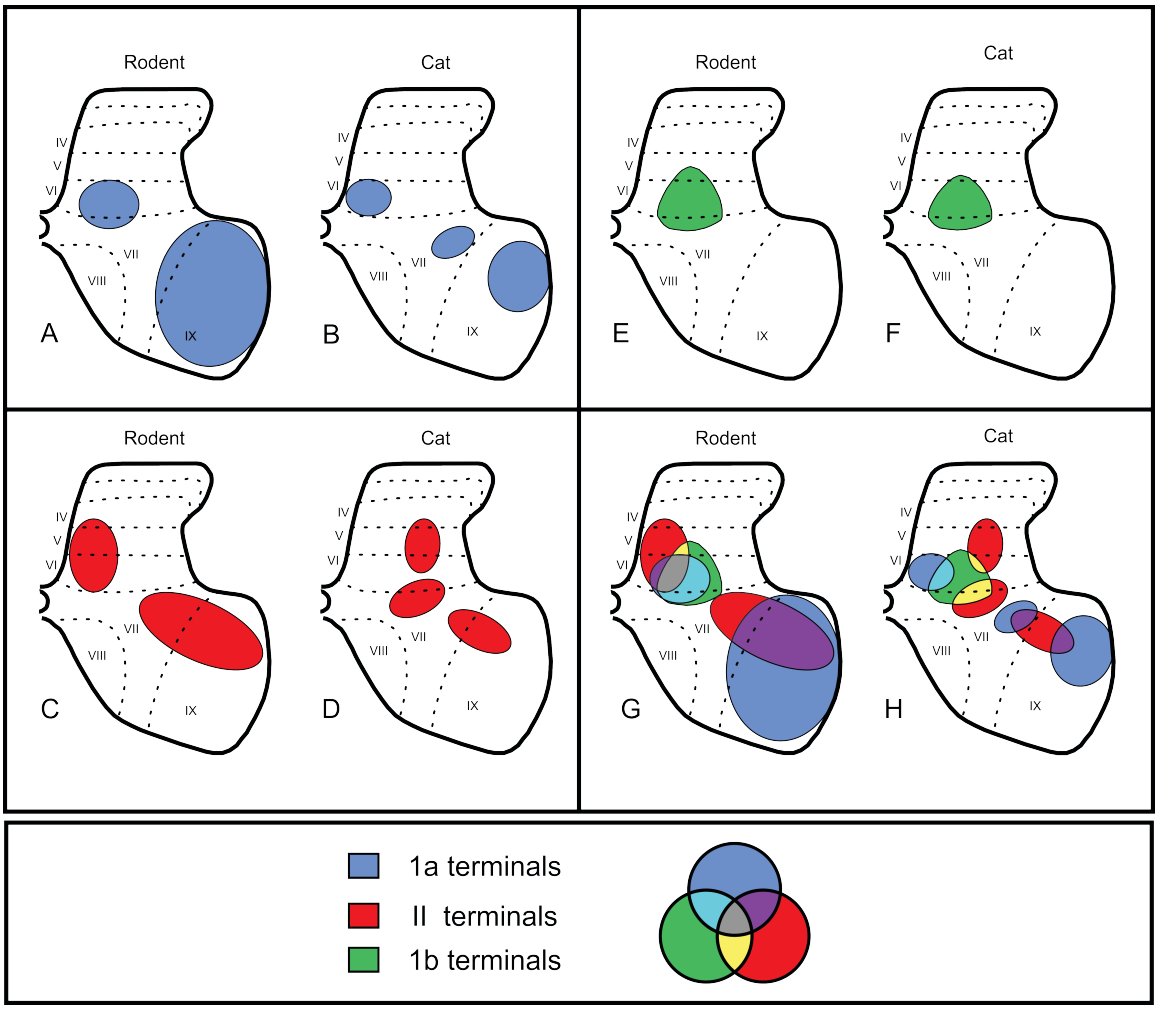
Rodent
Cat
Rodent
Cat
IV
V
VI
VII
VIII
IX
A
B
E
F
Rodent
Cat
Rodent
Cat
C
D
G
H
1a terminals
II terminals
1b terminals

Figure 5. Diagrammatic representation of the average extent (distribution) of Ia, group II and Ib afferents throughout its corresponding target lamina in the rat triceps surae and cat lateral gastrocnemius/soleus. Figures representing cat afferents were adapted from A.G. Brown 1981, pg. 194. Color wheel demonstrates resulting colors from overlap between corresponding afferent types. Rat (A,E,C,G) and cat (B,F,D,H) afferent collateral share comparable trajectories and target lamina within each afferent class. However, the two mammalian models demonstrate noticeable differences in their average distribution of terminal arborizations within each target laminae.

TABLE 1

ble 1. *Average number of Neurobiotin-filled synaptic varicosities in target laminae per 75 µm section*

	1a*			Group II			Ib		
amina(s)	**Afferent 1**	**Afferent 2**	**Afferent 3**	**Afferent 4***	**Afferent 5**	**Afferent 6**	**Afferent 7**	**Afferent 8**	**Afferent 9**
IV - VI	**23.81 ± 42.64**	**8.71 ± 12.23**	**12.79 ± 19.64**	**24.33 ± 29.41**	**45.6 ± 43.70**	**24.78 ± 26.76**	**45.17 ± 42.87**	**38.91 ± 38.78**	**36.13 ± 37.04**
max	205.00	48.00	101.00	100.00	153.00	81	146.00	143.00	112.00
VII	**5.83 ± 11.48**	**4.85 ± 7.64**	**7.33 ± 11.29**	**11.37 ± 14.43**	**10.6 ± 19.12**	**4.26 ± 8.61**	**2.75 ± 6.10**	**5.81 ± 9.58**	**1.93 ± 4.31**
max	49.00	23.00	49.00	49.00	72.00	34.00	26.00	34.00	13.00
LIX	**19.95 ± 26.18**	**21.47 ± 27.93**	**19.98 ± 22.87**	**25 ± 37.36**	**5.95 ± 11.51**	**14.43 ± 16.31**	**0.00**	**0.00**	**0.00**
max	105.00	92.00	91.00	175.00	46.00	54.00			

ılues are mean ± SD per 75 µm section. The minimum number of contacts in each lamina was aways = 0

All Neurobiotin-filled varicosites verified by VGLUT1 content

TABLE 2

Table 2. *Average number of Neurobiotin-filled synaptic varicosities verified by VGLUT1 content*

	Group II			Ib		
Lamina(s)	**Afferent 4**	**Afferent 5**	**Afferent 6**	**Afferent 7**	**Afferent 8**	**Afferent 9**
IV - VI	**24.33 ± 29.41**	**22.45 ± 21.72**	**14.09 ± 17.44**	**40.84 ± 35.81**	**33.86 ± 31.85**	**15.13 ± 24.37**
max	100.00	82.00	67	118.00	135.00	84.00
VII	**11.37 ± 14.43**	**6.8 ± 13.40**	**3.52 ± 7.91**	**2.64 ± 5.99**	**5.82 ± 9.58**	**0.69 ± 2.75**
max	49.00	55.00	33.00	26.00	34.00	11.00
LIX	**25 ± 37.36**	**5.45 ± 9.77**	**13.74 ± 15.64**	**0.00**	**0.00**	**0.00**
max	175.00	36.00	54.00			

Values are mean ± SD per 75 μm section. The minimum number of contacts in each lamina was aways = 0